JOURNAL OF AIRCRAFT
Vol. 46, No. 2, March–April 2009

Engineering Notes

ENGINEERING NOTES are short manuscripts describing new developments or important results of a preliminary nature. These Notes should not exceed 2500 words (where a figure or table counts as 200 words). Following informal review by the Editors, they may be published within a few months of the date of receipt. Style requirements are the same as for regular contributions (see inside back cover).

Comparison of Theoretical Structural Models with Experiment for a High-Aspect-Ratio Aeroelastic Wing

Justin W. Jaworski* and Earl H. Dowell†
Duke University, Durham, North Carolina 27708

DOI: 10.2514/1.39244

Nomenclature

A_n	=	normalization factor
b	=	spar width
d_N	=	notch depth nondimensionalized by $b/2$
E	=	elastic modulus
f	=	frequency [Hz]
I_x	=	tip store torsional inertia
I_1, I_2	=	flapwise, chordwise area moments
K	=	average wing radius of gyration
L	=	wingspan
M	=	tip store mass
m	=	average mass per unit length of the wing
t	=	spar thickness
x	=	spanwise position coordinate nondimensionalized by L

Subscripts

nB	=	nth out-of-plane bending mode
nC	=	nth in-plane bending mode
nT	=	nth torsion mode
ub	=	uniform beam value

Symbols

β_n	=	nth torsional eigenvalue
Θ_n	=	nth torsional mode shape
λ_n	=	nth bending eigenvalue
χ_n	=	nth flapwise mode shape
ψ_n	=	nth chordwise mode shape

Introduction

MATERIALS of various densities and stiffnesses typically constitute the experimental slender wing structures designed for flutter and limit cycle oscillation experiments of high-altitude long-endurance (HALE) aircraft. Recent research performed at Duke University includes a study inter alia of the effects of structural nonuniformity on the natural frequencies and mode shapes of very flexible beams, which are frequently used in geometrically nonlinear structural analyses of HALE wings [1–5]. Jaworski and Dowell [6] demonstrated that such beamlike structures with spanwise discontinuities could be represented modally as a uniform beam for sufficiently small spanwise discontinuities. However, determining the set of natural frequencies requires knowledge of any such discontinuities or variations.

This work addresses the effects of these nonuniformities on the four lowest natural frequencies of a cantilevered HALE-type wing. Here, the experimental wing model used by Tang and Dowell [2–4] is analyzed using the commercial finite element program ANSYS. As shown in Fig. 1, the HALE wing is composed of a steel spar with multiple steps, periodically-spaced aluminum ribs, balsa wood fairings to fill the space between ribs, and a tip store. Specifically, the effects examined herein are the step depth for the particular step distribution used by Tang and Dowell [2–4]; the addition of periodically-spaced ribs; the presence of balsa wood fairings with varying levels of rigid connection to the central spar; and the addition of a tip store.

Model Results and Discussion

For this study the total spar length, maximum width, thickness, step distribution, and step width are held constant; only the step depth varies. Step depth is defined as the chordwise dimension of material removed symmetrically from the spar, which is 3.17 mm for the model in Fig. 1b. The step depth is scaled by the spar half-width, and the natural frequencies by their uniform beam values of the spar alone, f_{ub}. The four natural frequencies of interest ($f_{1B}, f_{2B}, f_{1C}, f_{1T}$) are tracked as the nondimensional step depth d_N varies.

The physical parameters used in the finite element computations for balsa wood, aluminum, and steel are $\rho = 138.5$, 2664, and 4850 kg $\cdot$ m^{-3}; $E = 2.34$, 60.6, and 200 GPa; and $\nu = 0.3$, 0.33, and 0.3, respectively. The densities are calculated from total mass and dimensional data of material specimens, and the elastic moduli are calibrated to their first flapwise resonance using classical beam theory. Standard handbook values are assumed for the Poisson ratios.

All figures herein indicate actual finite element data with symbols unless otherwise noted, and the curves between these symbols are interpolated using piecewise cubic splines [7]. The results are analyzed for individual additions of ribs, fairings, and a tip store, as well as their combined effects on natural frequencies.

Step Depth

The spar is modeled using two-dimensional, eight-node structural shell elements (SHELL93) [8]. The finite element meshes are generated by the SmartSizing free-meshing function within ANSYS, set to the highest possible resolution.

The natural frequency results in Fig. 2 show that the first two out-of-plane bending mode trends are virtually coincident, and that the torsion mode follows a very similar trend. This similarity is anticipated because both torsional and out-of-plane bending stiffnesses scale as bt^3. The frequency trend for the in-plane bending mode is an almost linear function of the step depth, as expected from uniform beam theory where the in-plane stiffness scales as b^3t.

Received 20 June 2008; revision received 11 November 2008; accepted for publication 11 November 2008.

*Research Assistant, Department of Mechanical Engineering and Materials Science. Student Member AIAA.

†William Holland Hall Professor, Department of Mechanical Engineering and Materials Science. Honorary Fellow AIAA.

a)

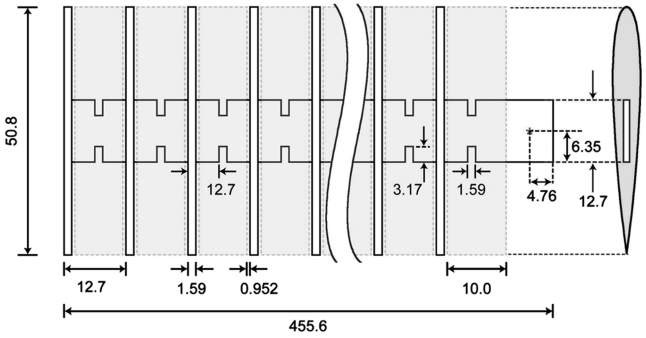

b)

Fig. 1 Aeroelastic wing with tip store: a) experimental model and b) schematic of the ANSYS model. Tip mass spanwise location is indicated by *. Dimensions are in millimeters.

Ribs

The effect of adding aluminum ribs with a NACA 0012 profile [9] is evaluated using both two-dimensional shell (SHELL93) and three-dimensional solid (SOLID45) finite element models. As shown in Fig. 3, the two- and three-dimensional finite element models are in close agreement, which suggests that three-dimensional effects at the constraints between the ribs and spars may be neglected.

A comparison between Figs. 2 and 3 indicates that rib addition does not change the qualitative frequency trends observed for the stepped spar, but rather the ribs change the magnitude of the results. The bending mode results are roughly 85% of those for the spar alone, whereas the torsion mode results are reduced by nearly 40%. Clearly, the main contribution of the ribs is an increase in torsional inertia.

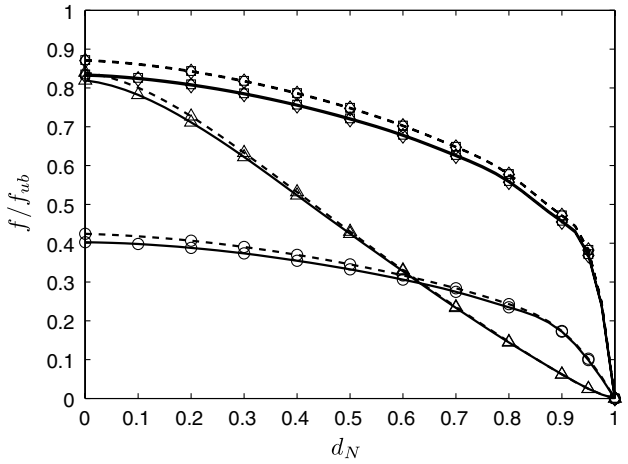

Fig. 3 Natural frequencies of spar with ribs as step depth is varied: solid line, 2-D; dashed line, 3-D. □, f_{1B}; ◇, f_{2B}; △, f_{1C}; and ○, f_{1T}.

Balsa Wood Fairings

This section addresses the addition of balsa wood fairings and the constraint conditions between the spar and fairings using three-dimensional solid elements. Figure 4 shows that the fairings dominate the torsion and out-of-plane bending modes and that the step depth has virtually no effect. Therefore, the balsa wood addition acts effectively as a stiffness increase for the out-of-plane bending modes and an inertial increase for the torsion mode.

The particular distribution of balsa wood provides a modest 5% change in the natural frequency of the in-plane bending mode for zero step depth. The in-plane bending mode trend resembles that of the spar alone but approaches a nonzero frequency as $d_N \to 1$; the other modes also have nonzero frequencies in this limit because the balsa wood holds the structure together. It is also inferred from the limit $d_N \to 1$ that the presence of the balsa wood accounts for a quarter of the effective in-plane bending stiffness, recalling $f^2 \sim EI_2$.

The computations for the results shown in Fig. 4 assume that the balsa wood and spar are perfectly joined, i.e., the interfacial node displacements are identical. To investigate the influence of the compatibility condition, three alternative constraint conditions are considered in the computational model for single- and double-component segments of the full structure.

First, the constraint between the fairings and spar is relaxed (i.e., stiffness due to shear flow is eliminated) along the thin edges of the

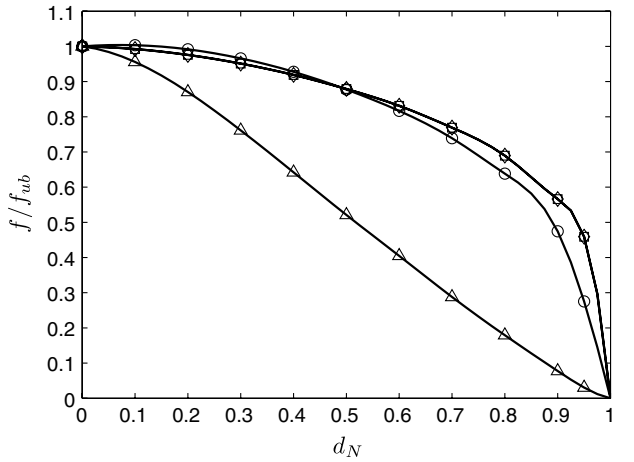

Fig. 2 Spar natural frequencies as step depth is varied: □, f_{1B}; ◇, f_{2B}; △, f_{1C}; and ○, f_{1T}.

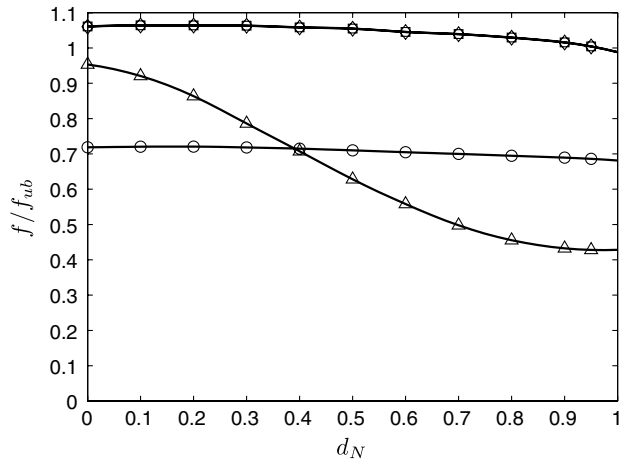

Fig. 4 Natural frequencies of 3-D spar with balsa wood fairings as step depth is varied: □, f_{1B}; ◇, f_{2B}; △, f_{1C}; and ○, f_{1T}.

spar; this effect is very small (∼1%) for all modes. Second, the constraint along the wide edges of the spar is relaxed instead. The in-plane bending mode is relatively unchanged, but the out-of-plane bending and torsion values decrease by roughly 5–10%. However, the comparison of component results suggests that the first out-of-plane natural frequency becomes progressively lower than the corresponding perfectly joined cases, whereas the second out-of-plane bending and torsion natural frequencies have a relative increase. The stiffening of the second bending mode for the double-component case is thought to explain its trend difference from the first out-of-plane mode.

Third, the balsa wood fairings are connected to the spar only at its outermost corner points using constraint equations to relate node displacements. The net effect is a limiting case where the balsa wood is solely a mass addition. The in-plane bending and torsion results are most affected. The change in out-of-plane natural frequencies is roughly 5–10%, though more data would be needed to deduce a trend because the constraint locations and node lines of the bending modes factor significantly into the analysis. This was a lesser concern for the other cases because the constraint was applied over an area instead of at a small number of points.

Overall, the effect of varying the compatibility conditions is modest for the in- and out-of-plane bending modes, but more pronounced for the torsion mode.

Tip Store

This section examines the three-dimensional spar when fitted with a tip store. The store is modeled as two identical point masses positioned such that the effective mass and torsional inertia match the measured values of $M = 36.95$ g and $I_x = 8.314 \times 10^{-5}$ kg · m^2, respectively.

The results in Fig. 5 show that the tip store inertia renders the torsional mode almost insensitive to step depth. Also, the bending mode trends are similar to those of the spar alone. For the first time, the out-of-plane bending mode curves do not overlap because the frequency results depend on the tip store placement relative to the nodes of the particular mode shape.

Combined Effects

The modeling variations analyzed herein are now combined to observe their net effect on the natural frequencies. Figures 6–9 describe the frequency behavior of the stepped spar as the ribs, balsa wood fairings, and tip store are added in sequence.

The trends are similar for the out-of-plane bending and torsion modes. The addition of the ribs reduces the magnitude of the stepped spar frequency results to varying degrees, which indicates that the ribs essentially contribute more inertia than stiffness. Balsa wood fairings flatten the curve and increase the frequency values, indicating that the fairing stiffness dominates and that step depth

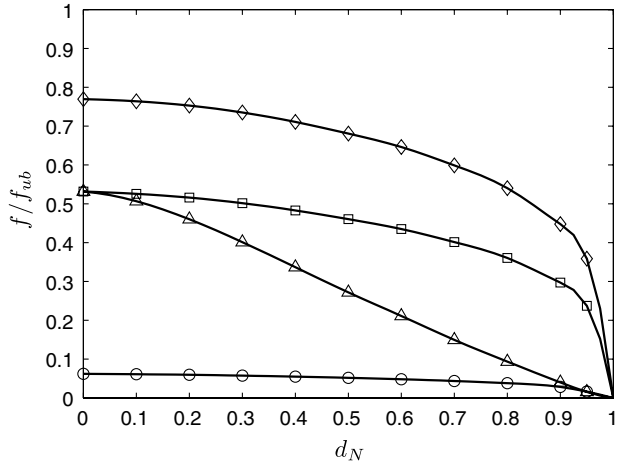

Fig. 5 Natural frequencies of 3-D spar with a tip store as step depth is varied: □, f_{1B}; ◇, f_{2B}; △, f_{1C}; and ○, f_{1T}.

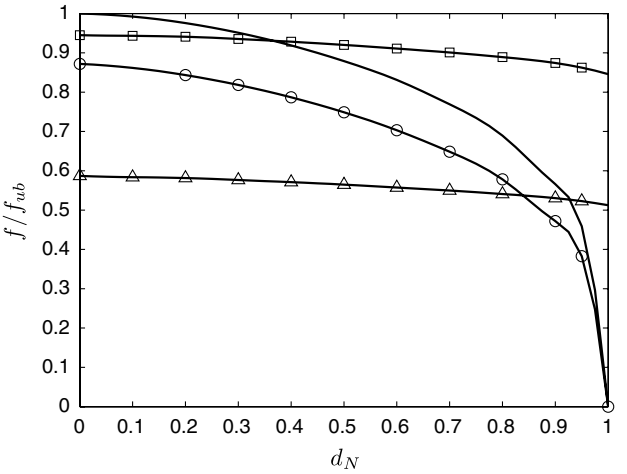

Fig. 6 Combined effects on f_{1B} for varying step depth: solid line, spar alone; ○, with ribs; □, with ribs and fairings; and △, with ribs, fairings, and tip store.

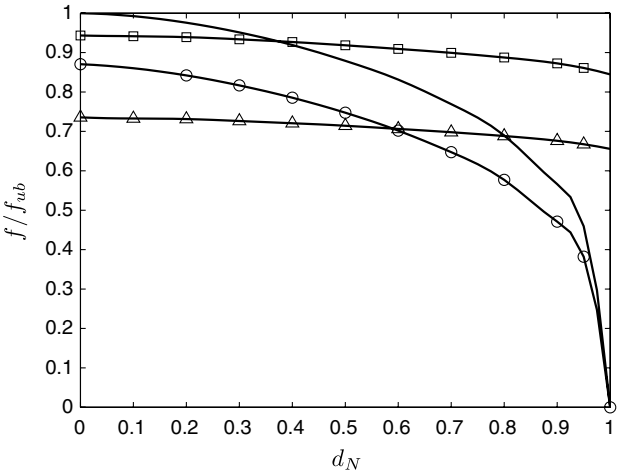

Fig. 7 Combined effects on f_{2B} for varying step depth: solid line, spar alone; ○, with ribs; □, with ribs and fairings; and △, with ribs, fairings, and tip store.

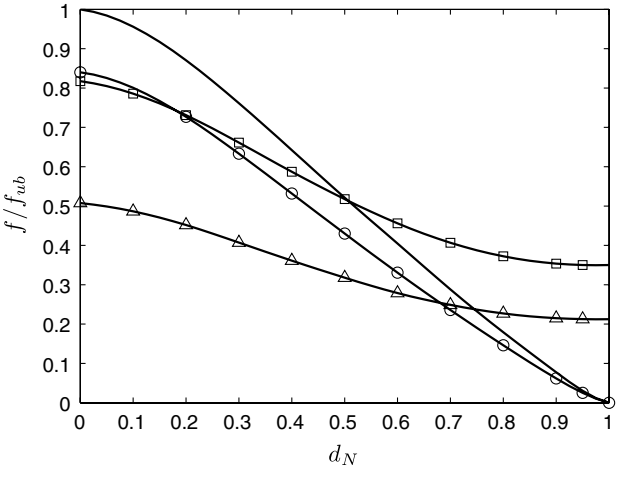

Fig. 8 Combined effects on f_{1C} for varying step depth: solid line, spar alone; ○, with ribs; □, with ribs and fairings; and △, with ribs, fairings, and tip store.

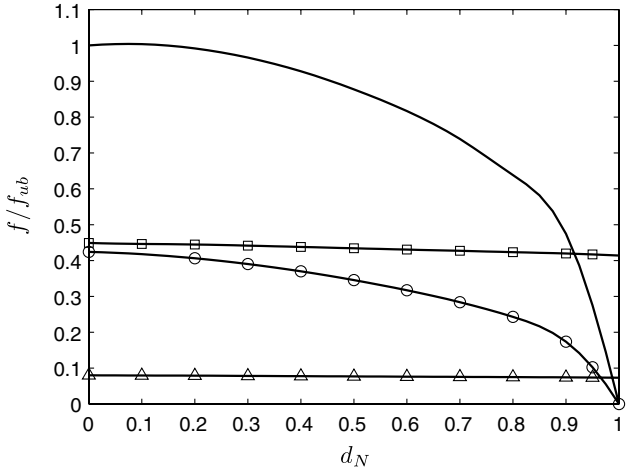

Fig. 9 Combined effects on f_{1T} for varying step depth: solid line, spar alone; ○, with ribs; □, with ribs and fairings; and △, with ribs, fairings, and tip store.

effects become less important. The tip store affects the curves such that the final configuration has out-of-plane bending and torsion frequencies lower than those of the spar alone. The resulting out-of-plane bending and torsion modes are effectively independent of step depth.

The change in the in-plane bending mode frequency behavior in Fig. 8 is less pronounced than for the other modes. The rib addition changes the uniform spar frequency by 15%, a difference that diminishes as the step depth is increased. The subsequent balsa wood addition retains the uniform spar trend but changes the frequency for $d_N \to 1$ to a nonzero value as with the other modes. The tip store scales down the magnitude of previous results as seen with the other modes.

Table 1 Comparison of ANSYS and experimental natural frequencies for $d_N = 0.5$

Mode	ANSYS		Experiment	
	Without store	With store	Without store	With store
f_{1B}	4.598 (3.968)[a]	2.882 (2.658)	4.000	2.625
f_{2B}	28.76 (24.83)	22.37 (19.87)	22.38	17.88
f_{1C}	25.82 (22.29)	15.86 (14.93)	23.13	14.13
f_{1T}	145.3 (140.9)	25.75 (25.71)	102.9	22.88

[a]Parentheses values indicate the total mass matched to the experiment.

The results shown in Figs. 6–9 support the hypothesis that an aeroelastic wing could be designed by varying the tip store properties and step depth alone. Explicitly, the out-of-plane bending modes depend primarily on the tip store mass; the tip store mass and step depth tune the in-plane bending frequency; and tip store torsional inertia controls the torsion frequency. The next section validates such frequency design curves against experiment.

Theoretical–Experimental Comparison

The HALE-type wing [2–4] natural frequencies were measured using a transducer-fitted impact hammer [Brüel & Kjær (B&K) type 8204] and an accelerometer (B&K type 4374). The signal from the accelerometer is boosted by a charge amplifier (B&K type 2635), and the transfer function between the hammer and accelerometer is measured by the B&K PULSE data acquisition system. Each transfer function is averaged linearly over five impacts at the spar tip. Every impact is sampled at 256 Hz for 8 s, yielding a frequency resolution of 125 mHz.

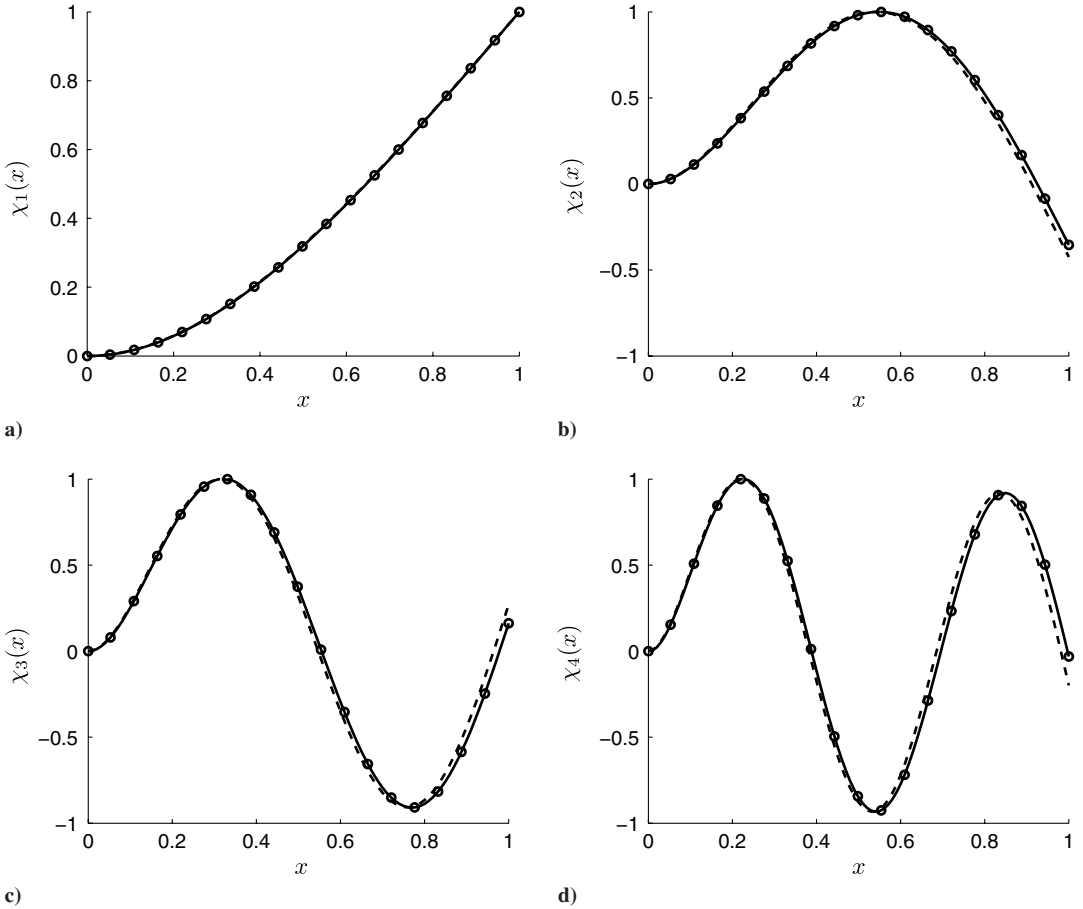

Fig. 10 Flapwise mode shapes for HALE wing with tip store: a) χ_1; b) χ_2; c) χ_3; d) χ_4. ○, ANSYS data; solid line, least-squares polynomial fit of ANSYS data; and dashed line, uniform beam theory.

Table 1 compares the results for the three-dimensional finite element model both with and without the tip store with observed values for the HALE-type wing. Without the tip store, the finite element model agrees to within 15–30% of comparable experimental values for the bending modes. Lesser agreement is observed for the torsion mode. The full model with tip store overestimates the experimental values by roughly 10–25%; the second out-of-plane mode has the largest overestimate.

The results for the mass-corrected model are placed in parentheses for Table 1. The ANSYS bending mode results agree to within 11% of experiment using the mass correction. The torsion mode is virtually unaffected because the assumed radius of gyration of the added mass is small.

Mode Shapes

This section compares the mode shapes of uniform beam theory to those from the finite element wing model for $d_N = 0.5$, which corresponds to the experimental wing in Ref. [2] (cf. Fig. 1). This comparison demonstrates how accurately the present three-dimensional HALE wing finite element model with its many nonuniformities can be approximated by classical beam theory.

Figures 10–12 compare the wing mode shapes with the tip store. The ANSYS modal deflections are recorded for 18 spanwise locations at the midchord, and a least-squares 10th-order polynomial curve fit is drawn through the data. The classical bending modes are described by

$$\chi_n(x), \psi_n(x) = A_n\left[(\cos\lambda_n x - \cosh\lambda_n x) - \left(\frac{\cos\lambda_n + \cosh\lambda_n}{\sin\lambda_n + \sinh\lambda_n}\right)(\sin\lambda_n x - \sinh\lambda_n x)\right] \tag{1}$$

where A_n is a scaling factor to normalize the mode shape, and λ_n are solutions to the transcendental equation [10]

$$1 + \cos\lambda_n \cosh\lambda_n = \lambda_n\left(\frac{M}{mL}\right)(\sin\lambda_n \cosh\lambda_n - \cos\lambda_n \sinh\lambda_n) \tag{2}$$

The torsion mode shape is $\Theta_n(x) = A_n \sin(\beta_n x)$, where β_n satisfies [10,11]

$$\beta_n \tan\beta_n = \frac{mLK^2}{I_x} \tag{3}$$

To compare the mode shapes directly, the values $M/mL = 0.4032$ and $mLK^2/I_x = 9.496 \times 10^{-2}$ follow from the ANSYS model. Classical theory closely approximates the resulting ANSYS mode shapes when including tip store effects, especially for the higher-order flapwise modes in Fig. 10. The first modes remain virtually coincident without the tip store, but the maximum percentage differences between the second-, third-, and fourth-order flapwise modes grow to 5.38, 9.72, and 13.5%, respectively.

Overall, the finite element mode shapes of the considered nonuniform HALE wing model are well-described by classical uniform beam theory. The addition of a tip store improves the approximation of the computed mode shapes by classical theory.

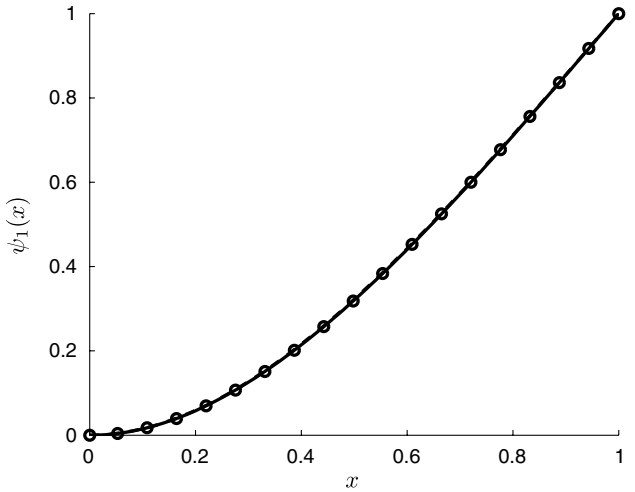

Fig. 11 First chordwise mode shape for HALE wing with tip store: ○, ANSYS data; solid line, least-squares polynomial fit of ANSYS data; and dashed line, uniform beam theory.

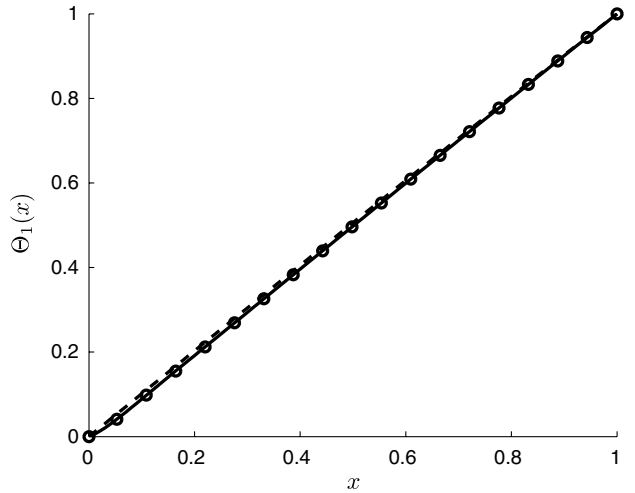

Fig. 12 First torsion mode shape for HALE wing with tip store: ○, ANSYS data; solid line, least-squares polynomial fit of ANSYS data; and dashed line, uniform beam theory.

Conclusions

A computational structural analysis is performed for a high-aspect-ratio, experimental aeroelastic wing model using the commercial finite element program ANSYS. The computational results quantify the effects of spanwise nonuniformities such as ribs, fairings, and a tip store on the first four wing modes. The mode shapes of the nonuniform finite element wing model are shown to be well-approximated by classical beam modes, which are typically assumed as trial functions for nonlinear aeroelastic analyses of slender wings. In addition, the computed natural frequency results are compared with those from experiment and shown to be in reasonable agreement. The agreement between computational and experimental results without resorting to empiricism supports the use of ANSYS as a design tool for aeroelastic analyses of HALE-type wings.

References

[1] Dunn, P., and Dugundji, J., "Nonlinear Stall Flutter and Divergence Analysis of Cantilevered Graphite/Epoxy Wings," *AIAA Journal*, Vol. 30, No. 1, Jan. 1992, pp. 153–162.

[2] Tang, D. M., and Dowell, E. H., "Experimental and Theoretical Study on Aeroelastic Response of High-Aspect-Ratio Wings," *AIAA Journal*, Vol. 39, No. 8, Aug. 2001, pp. 1430–1441.

[3] Tang, D. M., and Dowell, E. H., "Experimental and Theoretical Study of Gust Response for High-Aspect-Ratio Wing," *AIAA Journal*, Vol. 40, No. 3, March 2002, pp. 419–429.

[4] Tang, D. M., and Dowell, E. H., "Limit-Cycle Hysteresis for a High-Aspect-Ratio Wing Model," *Journal of Aircraft*, Vol. 39, No. 5, Sept.–Oct. 2002, pp. 885–888.

[5] Tang, D. M., and Dowell, E. H., "Effects of Geometric Structural Nonlinearity on Flutter and Limit Cycle Oscillations of High-Aspect-Ratio Wings," *Journal of Fluids and Structures*, Vol. 19, No. 3, Apr. 2004, pp. 291–306.

[6] Jaworski, J. W., and Dowell, E. H., "Free Vibration of a Cantilevered Beam with Multiple Steps: Comparison of Several Theoretical Methods with Experiment," *Journal of Sound and Vibration*, Vol. 312, Nos. 4–5, May 2008, pp. 713–725.

[7] MATLAB, Software Package, Ver. 7.1.0,The Mathworks, Inc., Natick, MA, 2005.
[8] ANSYS, Software Package, Ver. 10.0, ANSYS, Inc., Canonsburg, PA, 2005.
[9] Abbott, I. H., and von Doenhoff, A. E., *Theory of Wing Sections*, 1st ed., McGraw–Hill, New York, 1949.
[10] Jaworski, J. W., "Ritz Analysis for Nonuniform Beam Models of High Aspect Ratio Wings," M.S. Thesis, Duke Univ., Durham, NC, 2006.
[11] Bisplinghoff, R. L., Ashley, H., and Halfman, R. L., *Aeroelasticity*, 1st ed., Dover, New York, 1996.